

Super-Resolution Based Patch-Free 3D Medical Image Segmentation with Self-Supervised Guidance

Hongyi Wang, Lanfen Lin, *Member, IEEE*, Hongjie Hu, Qingqing Chen, Yinhao Li, Yutaro Iwamoto, *Member, IEEE*, Xian-Hua Han, Yen-Wei Chen, *Member, IEEE*, and Ruofeng Tong

Abstract—High resolution (HR) 3D medical image segmentation plays an important role in clinical diagnoses. However, HR images are difficult to be directly processed by mainstream graphical cards due to limited video memory. Therefore, most existing 3D medical image segmentation methods use patch-based models, which ignores global context information that is useful in accurate segmentation and has low inference efficiency. To address these problems, we propose a super-resolution (SR) guided patch-free 3D medical image segmentation framework that can realize HR segmentation with global information of low-resolution (LR) input. The framework contains two tasks: semantic segmentation (main task) and super resolution (auxiliary task). To balance the information loss with the LR input, we introduce a Self-Supervised Guidance Module (SGM), which employs a selective search method to crop a HR patch from the original image as restoration guidance. Multi-scale convolutional layers are used to mitigate the scale-inconsistency between the HR guidance features and the LR features. Moreover, we propose a Task-Fusion Module (TFM) to exploit the inter connections between segmentation and SR task. This module can also be used for Test Phase Fine-tuning (TPF), leading to a better model generalization ability. When predicting, only the main segmentation task is

This work was supported in part by the Natural Science Foundation of Zhejiang Province (LZ22F020012) and Major Scientific Research Project of Zhejiang Lab (2020ND8AD01). This work was also supported by the National Natural Science Foundation of China (82071988), the Key Research and Development Program of Zhejiang Province (2019C03064), and in part by the Grant in Aid for Scientific Research from the Japanese Ministry for Education, Science, Culture and Sports (MEXT) under the Grant No. 20KK0234, No. 21H03470, and No. 20K21821. (Corresponding authors: Lanfen Lin; Hongjie Hu; Yen-Wei Chen.)

Hongyi Wang is with the College of Computer Science and Technology, Zhejiang University, Hangzhou 310063, China (e-mail: whongyi@zju.edu.cn).

Lanfen Lin is with the College of Computer Science and Technology, Zhejiang University, Hangzhou 310063, China (e-mail: llf@zju.edu.cn).

Hongjie Hu is with the Department of Radiology, Sir Run Run Shaw Hospital, Hangzhou 310016, China (e-mail: hongjiehu@zju.edu.cn).

Qingqing Chen is with the Department of Radiology, Sir Run Run Shaw Hospital, Hangzhou 310016, China (e-mail: qingqingchen@zju.edu.cn).

Yinhao Li is with the Research Center for Healthcare Data Science, Zhejiang Laboratory, Hangzhou 311100, China (e-mail: lyh@zhejianglab.com).

Yutaro Iwamoto is with the College of Information Science and Engineering, Ritsumeikan University, Kusatsu 5250058, Japan (e-mail: yiwamoto@fc.ritsumei.ac.jp).

Xian-Hua Han is with the Artificial Intelligence Research Center, Yamaguchi University, Yamaguchi 7538511, Japan (e-mail: hanhua@yamaguchi-u.ac.jp).

Yen-Wei Chen is with the College of Information Science and Engineering, Ritsumeikan University, Kusatsu 5250058, Japan, also with the DUT-RU Co-Research Center of Advanced ICT for Active Life, Research Center for Healthcare Data Science, Zhejiang Laboratory, Hangzhou 311100, China, and also with the College of Computer Science and Technology, Zhejiang University, Hangzhou 310063, China (e-mail: chen@is.ritsumei.ac.jp).

Ruofeng Tong is with the College of Computer Science and Technology, Zhejiang University, Hangzhou 310063, China, and also with the Research Center for Healthcare Data Science, Zhejiang Laboratory, Hangzhou 311100, China (e-mail: trf@zju.edu.cn).

needed, while other modules can be removed to accelerate the inference. The experiments results on two different datasets show that our framework outperforms current patch-based and patch-free models. Our model also has a four times higher inference speed compared to traditional patch-based methods. Our codes are available at: <https://github.com/Dootmaan/PFSeg-Full>.

Index Terms—3D medical image segmentation, Patch-Free, Multi-task learning, Super resolution, Self-supervision.

I. INTRODUCTION

SEGMENTATION is one the most important tasks in medical image processing. Accurate lesion segmentation of high-resolution (HR) medical images has great significance for the diagnosis. Nowadays, Computer Aided Diagnoses (CAD) system has been developed to facilitate doctors in early detection and treatment of diseases. Traditional CAD system usually rely on hand-engineered features that limits its performance and accuracy. Therefore, many deep learning models have been proposed recently to achieve better performance for medical image segmentation. However, many medical images produced by Computed Tomography (CT) or Magnetic Resonance Imaging (MRI) are 3D volumetric data with high resolution that cannot be directly processed by most mainstream graphical cards. Thus, many previous works chose to split the entire data along the z-axis into 2D slices [1], [2], [3], [4], [5], and use these 2D slices to perform segmentation tasks separately. But such approaches ignore the valuable information among slices. As a result, to solve this problem, some 2.5D [6], [7] and 2D multiple views [8], [9], [10] methods are presented for the efficient use of such information. 2.5D methods partially learn 3D features by feeding multiple neighboring 2D slices as different channels into a 2D CNN network. Whereas 2D multiple view methods attempt to model 3D features with all the 2D features learned by 2D CNNs from different directions (i.e., axial, coronal, and sagittal). Despite that, both 2.5D and 2D multiple view are still 2D-based methods in essence and they do not fully utilize the 3D data.

In contrast, 3D convolution is more suitable for processing 3D images. However, due to limited GPU memory, most existing 3D segmentation methods are patch-based [11], [12], [13]. In patch-based scheme, the model receives only local patch information of an image at a time. Patch-based 3D segmentation methods can be considered as a divide-and-conquer method in which, first, each 3D medical image is divided into several small regions with a certain degree of

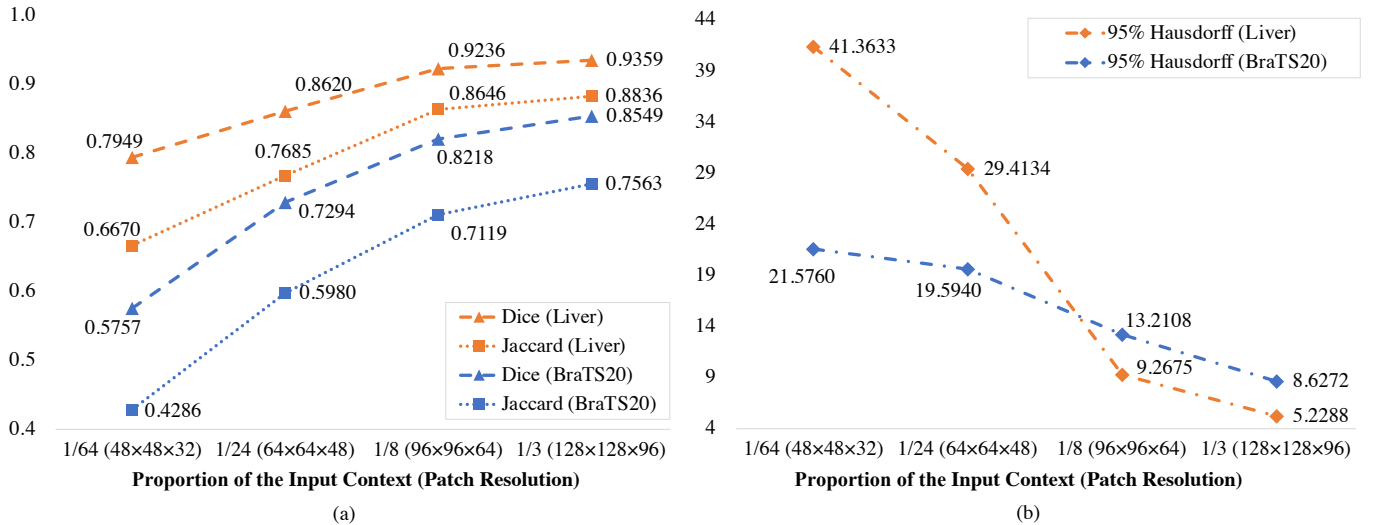


Fig. 1. (a) The Dice Similarity Coefficient, Jaccard Coefficient and (b) 95% Hausdorff Distance of different patch size using 3D Res-UNet on two datasets. As is shown, a bigger patch size with more context tends to have a better performance.

overlap. Second, a segmentation task is performed on each divided small region. Finally, the segmentation output results for each patch are fused together as the entire segmentation mask of the original image. With the use of patches, the training of 3D models becomes available for most mainstream graphical cards, but in this learning scheme, useful global information, which can play a significant role in identifying lesions, is lost.

Recently, the importance of global contextual information has been described in some studies [14], [15]. During our experiments, we tested a baseline 3D segmentation model with different patch sizes, and we found that methods using a patch that contains more context have superior performance. The results are shown in Fig. 1. According to the graphs, we observed that multiple metrics have improved as the contextual information increases. Besides, when used for inference, patch-based methods not only severely decrease the efficiency, but also reduce the model accuracy due to inconsistencies introduced during the fusion process between patches [15]. Therefore, a low cost 3D patch-free segmentation method is urgently needed.

In order to realize patch-free segmentation with a clinic-affordable computational cost, we propose a framework using down-sampled low-resolution (LR) images as input and generate the original-sized high-resolution (HR) segmentation masks. Inspired by [16], we introduce an auxiliary Super-Resolution task (SRT) to enhance the framework's capability of restoring HR representation from LR inputs. We also designed a Self-Supervised Guidance Module (SGM) to directly keep some HR features from a representative HR image patch. The guidance patch is selected using our carefully-designed selective searching algorithm, which can find the most informative patch with less time. A Multi-Scale Residual Block (MSRes Block) is used along with this module to mitigate the scale-inconsistency between the LR global-wise features and HR SGM features. In addition, we designed a

Task-Fusion Module (TFM) that integrates the segmentation task and the SR task together to optimize these tasks jointly. TFM enhances the ability of the network to retrieve high-frequency information in target region segmentation, resulting in more accurate HR segmentation. In our experiments, We observe that TFM can also be used for Test Phase Fine-tuning (TPF) to increase the generalization capability of our network.

Contributions: The goal of this study is to present a patch-free 3D medical image segmentation method with lower GPU memory consumption. Our primary contributions are summarized as follows:

- We propose a patch-free 3D medical image segmentation framework based on multi-task learning, which can realize HR segmentation with LR input. The proposed framework improves the performance with high inference efficiency in comparison to traditional patch-based models. This makes it more suitable for real-world clinical implementation.
- We propose a Multi-Scale Self-Supervised Guidance Module (SGM) to keep some HR features. This module uses a fast selective cropping algorithm to find a HR guidance patch as input to handle the high-frequency information loss of the LR input. In addition, SGM also optimizes the auxiliary SR task in a self-supervised manner, benefiting the overall framework.
- We design a Task-Fusion Module (TFM) to exploit the inter connections between the segmentation task and the SR task. This module fuses the two tasks together to optimize them jointly.
- We propose Test Phase Fine-tuning (TPF) to improve the generalization ability of the framework. TPF uses the available test set HR image as SRT ground truth to fine-tune the parameters of model. Specially, TPF has the best performance when combined with TFM.

A preliminary version of this work [17] was presented as a conference paper at MICCAI 2021, the 24th International

Conference on Medical Image Computing and Computer Assisted Intervention. This work provides substantial, conceptual and experimental studies including:

- 1) We propose a new Multi-Scale Residual Block (MSRes Block) for the encoder and SGM to mitigate the scale-inconsistency between HR guidance features and LR global-wise features.
- 2) We introduce selective cropping, an efficient guidance patch searching algorithm for SGM. This approach determines more informative HR patches than the previously proposed central cropping method, while maintaining a fast speed.
- 3) Here, we propose to use TFM for Test Phase Fine-tuning (TPF), which improves the generalization ability of our model.

The rest of the paper is organized as follows. Related works and their limitations are given in Section II. The detailed description of our proposed framework is presented in Section III along with the newly proposed works. Specifically, the improved MSRes Block is introduced in Section III.B2, and the selective cropping algorithm is described in Section III.B3. The proposed TPF is presented in Section III.D. Detailed experimental validation and results are reported in Section IV. Finally, our work is summarized and concluded in Section V.

II. RELATED WORKS

A. Deep Learning in Medical Image Segmentation

Nowadays, deep learning has been widely used in medical image segmentation. In 2015, Ronneberger et al. proposed U-Net for biomedical image segmentation [1]. Though it is still a Fully Convolution Network (FCN) with the classic encoder-decoder structure, it is a instrumental network introducing skip connections for the decoder. Skip connection reuses the features from the encoder by concatenating them with the features of decoder part. Employing skip connections, the decoder can use both low level and high level features for feature extraction. Since then, many works have been presented to improve the U-Net network, such as combining the attention mechanism [18] and residual connections [19].

Although U-Net alike models have achieved remarkable success on medical image segmentation, these networks only accept a single 2D image at a time. There have been many methods to use 2D networks on 3D medical images, including 2.5D and 2D multiple views. 2.5D methods utilize the characteristic that medical images have intensity on each voxel rather than the 3-channel RGB information. For segmentation, each 2D slice is fed into the network together with its neighboring slices as different channels. But this also makes the method not suitable for multi-modality and multi-phase datasets. The 2D multiple views method implements the idea of using 2D slices obtained from all three axes separately. However, the 2D multiple views segmentation is still performed on a 2D space for every axis. In addition, this method requires 3 times more time for each case than normal 2D methods, making it practically less efficient.

The more intuitive way to handle 3D images is using the 3D networks. The 2D convolution operations in the existing

network can be replaced with 3D convolution operations to form a 3D network. But the main problem is the dramatic increase in GPU memory consumption. There are usually two ways of solving this problem. One approach is to reduce the width and depth of a model to reduce the parameters, but this degrades the performance of the network. The second is decreasing the size of the input images, such as down-sampling the input spatial resolution or providing patch-level inputs by splitting the image into patches. In previous methods, patch-based segmentation is more commonly used.

B. Patch-based 3D Medical Image Segmentation

Due to the large computational cost of training modern 3D segmentation models with HR medical images, most graphical cards have no choice but to use patch-sampling to lower the GPU memory usage.

Several 3D methods are presented to date. 3D U-Net [20] is the extended version of the classic U-Net. It changes the 2D convolutions to 3D convolutions and reduces the depth and spatial dimensions of the feature maps. Later, V-Net [21] is proposed, incorporating residual blocks and Dice Loss to enhance the performance. Recently, there are also works adopting network architecture search (NAS) to medical image segmentation [22], [23], attempting to push the performance boundary beyond u-shaped models. Theoretically, these networks can be directly trained with 3D medical images (volumetric data) if the video memory is large enough. But in practical, with the limited computation resources, these methods have to use patch-sampling for training.

Patch-based methods ignore the global context information, since each time the model receives only a small part of the entire image. During inference, the fusion process between patches is also very time-consuming, because for each image we have to run the model several times to get the segmentation mask of every patch. Moreover, inconsistencies between the overlapping regions of the patch may also affect the accuracy [15].

To solve this problem in 2020, Kim et al. proposed to use a graph-cut algorithm-based post-processing for the 3D U-Net segmentation [24]. Their approach comparatively minimizes the segmentation errors caused by patch-sampling. However, since the input images still do not contain global context, performance of the network is limited. Kao et al. proposed a location information fusion method to solve the problem of patch-sampling. This approach uses existing brain parcellation atlases to embed location information into patch inputs [25]. Nonetheless, this method only focuses on the theoretical probability of lesions at different locations, and still cannot have the overall view of an image.

C. Patch-free 3D Medical Image Segmentation

To address the problems of patch-based methods, the design of efficient and accurate patch-free methods is required. Patch-free methods employs the entire contextual information of an image as input and make better prediction. They can also accelerate the predicting speed, since they process the 3D volumetric data information as an single input.

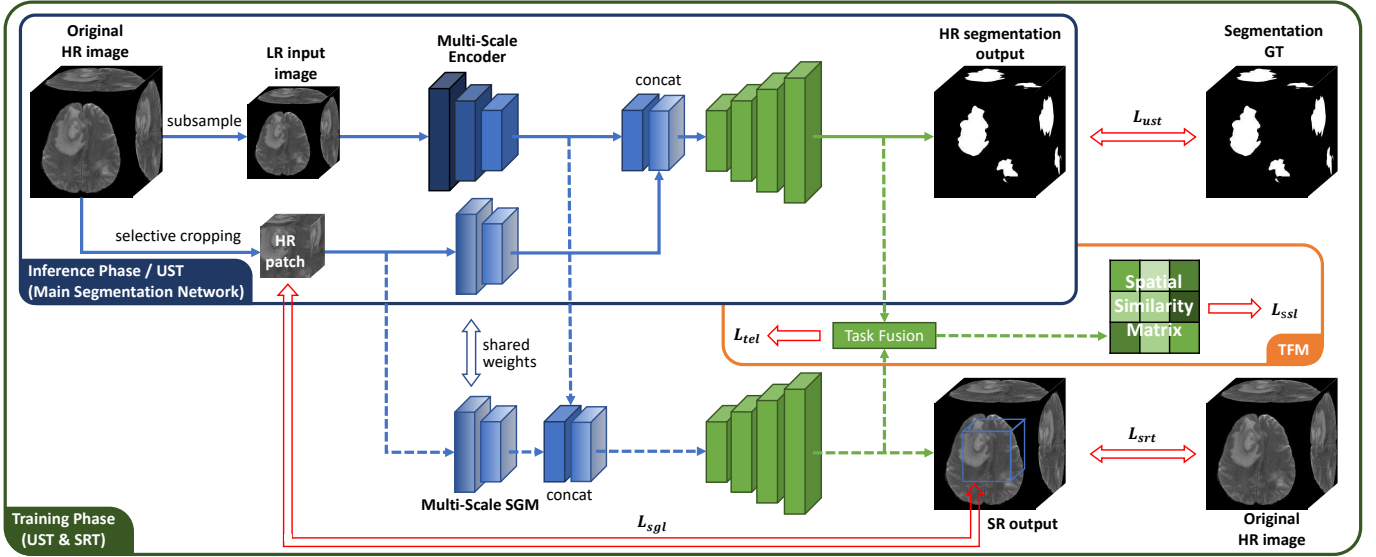


Fig. 2. A schematic view of the proposed framework. Different modules are labeled with different color. UST refers to Upsample-Segmentation Task and SRT denotes Super-Resolution Task. In the test phase, only the main segmentation network part (i.e., UST and its corresponding SGM) is needed. Best viewed in color.

However, if we do not reduce the width and depth of a model and sacrifice its performance, it will be hard to train the model with mainstream graphical cards. A naïve idea would be first down-sample the input and then use a full-sized 3D model to get a LR segmentation mask. After that, we can enlarge the mask to original image size with existing upsampling methods such as tricubic interpolation [26]. The drawback of this method is that it uses low-dimensional space to perform segmentation, resulting in the loss of valuable high-frequency details of the original image.

Unfortunately, so far there are only a few works focusing on patch-free segmentation. In 2019, Zeng et al. proposed Holistic Decomposition (HD) [14] for effective 3D medical image segmentation. Holistic Decomposition is the inverse operation of Sub-Pixel [27]. For a $W \times H \times D$ image, we can firstly use HD to decompose it into several small images and then use the concatenation of them as the 3D model's input. The decomposition process can be viewed as separating the voxels into different output channels with a certain order. By using this method, we can reduce the width and height of feature maps and still use all the input voxels. In the end, the final output mask is restored using Sub-Pixel operation. Though this method can achieve a good balance between inference speed and GPU memory cost, its performance is not so ideal because the network's width is reduced relatively. Later in 2021, Ho et al. used an ingenious way to realize patch-free segmentation by converting the problem into a point-cloud segmentation problem [28]. At first, the authors use a simple Saliency Attention Network (SAN) which takes the entire image as input to coarsely locate the main target area (e.g. potential lesion area). Since the network architecture is very simple, it can be easily trained without patch-sampling. Then, they designed a Context-Aware Sampling method to adaptively sample the image into points. The sampled points are dense in the main target area while sparse in other regions. After

sampling, the input information is effectively reduced and can be processed by a full-sized point-cloud segmentation network. Although it is a cleverly designed method, the framework includes two separated stages and cannot be trained in an end-to-end manner. Different from these previously proposed methods, in our work, we aim to design a Patch-Free Segmentation framework which effectively solves these problems.

III. PATCH-FREE SEGMENTATION FRAMEWORK

A schematic view of our framework is shown in Fig. 2. The proposed framework can directly generate HR segmentation mask with LR input. It is composed by a multi-task learning network, a Task-Fusion Module (TFM) and two Self-Supervised Guidance Modules (SGM). For a given 3D medical image, we first down-sample it by 2 times to generate the LR image. This LR image is used as primary inputs to segmentation network. In addition, we also crop a small patch from the original HR image as guidance to keep some representative high-frequency information. The extracted features of the HR guidance patch (output of SGM) are combined with the extracted features of LR image (output of encoder) and provided to the decoder parts. It should be noted that in the test phase, we only need the main segmentation part of the framework, including the segmentation branch of the multi-task network and its corresponding SGM. All the other modules can be removed to minimize the computational and memory cost.

A. Multi-task Learning Network

Multi-task Learning is the foundation of our framework. Multi-task Learning is generally used to model related tasks jointly. Normally, multi-task learning methods treat multiple tasks equally both in training phase and test phase. However, since we only focus on the HR segmentation task, we treat

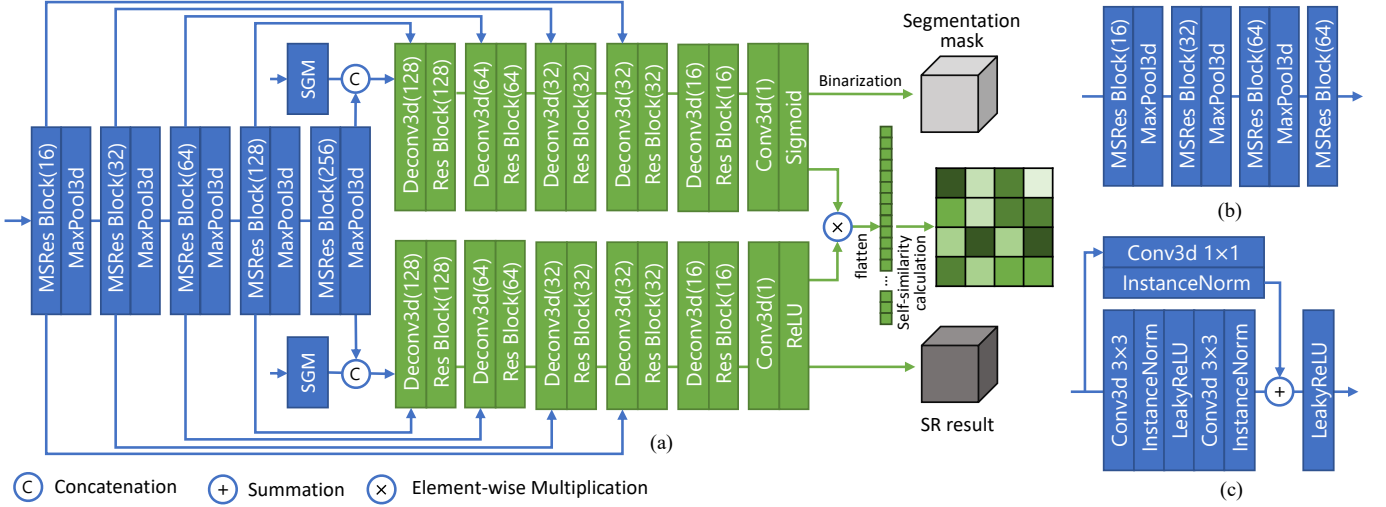


Fig. 3. (a) Detailed structure of the multi-task based framework. (b) Network structure of Self-Supervised Guidance Module (SGM). (c) Residual Block (Res Block) used in the framework.

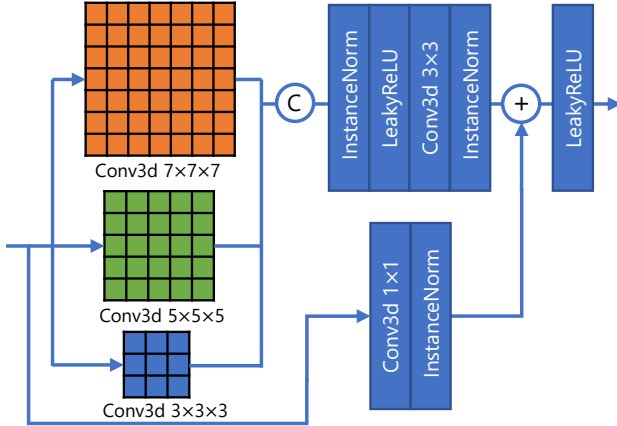


Fig. 4. Illustration of the Multi-Scale Residual Block (MSRes Block) used in the multi-scale encoder and SGM. This block has better modeling ability than the Res Block which is used in the decoders.

the segmentation task as main task and the SR task only as an auxiliary task.

To realize HR segmentation with LR input, firstly we need to append an up-sampling layer after the original segmentation backbone. The modified backbone will then be used to accomplish the so-called Upsample-Segmentation Task (UST). To help the segmentation model reconstruct the high-frequency feature maps from LR input image, we introduce Super-Resolution Task (SRT) as the second task. SRT can be considered as an auxiliary task and discarded in the inference stage. UST and SRT share the encoder. Whereas UST uses the segmentation mask as ground truth, SRT uses the original HR images as ground truth.

We have tested several different UST backbones. We select 3D Res-UNet [29] as the basis of our backbone to meet the balance between GPU memory cost and accuracy. 3D Res-UNet added residual connection [30] to the original 3D UNet, forming a Residual Block (Res Block) for each layer. We used five encoder layers, each one has a 32, 32, 64, 128

and 256 number of channels. The SRT branch has many optional network structures, but in our experiments, we found that using the same structure of the UST can achieve the best performance due to better structure consistency. The consistency between the structures of UST and SRT is quite important, since the two tasks share an encoder and will be fused together in TFM. The detailed structure of the Multi-task Learning network is shown in Fig. 3(a).

The loss function of this part can be divided into two parts. One is UST loss L_{ust} , which consists of Binary Cross Entropy (BCE) Loss and Dice Loss. Another one is SRT loss L_{srt} , which is a Mean Square Error (MSE) Loss. They can be formulated as:

$$L_{srt} = \frac{1}{N} \sum_{i=1}^N \|SRT(X \downarrow)_i - X_i\|^2, \quad (1)$$

$$L_{ust} = L_{bce} + L_{dice}, \quad (2)$$

and

$$L_{bce} = \frac{1}{N} \sum_{i=1}^N [-y_i \log(p_i) - (1 - y_i) \log(1 - p_i)], \quad (3)$$

$$L_{dice} = 1 - \frac{2 \sum_{i=1}^N P_i y_i}{\sum_{i=1}^N P_i^2 + \sum_{i=1}^N y_i^2}, \quad (4)$$

where N refers to the total number of all voxels, while X and $X \downarrow$ denote the original medical image and the down-sampled image respectively. $SRT(\cdot)$ represents the SRT branch output, while p_i and y_i are predicted probability of segmentation and the corresponding category for i -th pixel. It should also be noted that different from p_i , P_i denotes the prediction of i -th voxel after binarization.

B. Multi-Scale Self-Supervised Guidance Module

B1. Self-Supervised Guidance Module. For effective and better utilization of HR image, we propose Self Supervised

Module (SGM). SGM accepts a representative patch from the HR image as input, and extracts HR features from it. The extracted features are then concatenated with the output features of the shared encoder. The two SGM for UST and SRT (UST-SGM and SRT-SGM) share the parameters. However, in test phase, only the SGM for UST (i.e. UST-SGM) remains and the other one (i.e. SRT-SGM) is discarded. The detailed structure of SGM is presented in Fig. 3(b). The design of the SGM is very concise and the module accounts for only 5% of the total parameters of the network.

Let F_{share} and F_{sgm} represent the LR global-wise feature and the HR guidance feature. We can then describe the process as:

$$F_{share} = Encoder(X \downarrow), \quad (5)$$

$$F_{sgm} = SGM(X_{patch}), \quad (6)$$

$$O_{ust} = Decoder_{ust}(Concat(F_{share}, F_{sgm})), \quad (7)$$

$$O_{srt} = Decoder_{srt}(Concat(F_{share}, F_{sgm})), \quad (8)$$

where X_{patch} is the guidance patch cropped from the original HR image, while O_{srt} and O_{ust} represent the output of SRT and UST respectively.

B2. Multi-Scale Residual Block. It should be noted that the LR input image and HR guidance patch are of different scales. Hence, we introduce multi-scale design to solve this problem. The multi-scale convolutional layer is an updated form of the original Res Block used in 3D Res-UNet, and we call it Multi-Scale Residual Block (MSRes Block). MSRes Block fully inherits the modeling ability of the previous Res Block, meanwhile having a better capability of multi-scale feature learning. It is useful for mitigating the scale-inconsistency problem introduced during the concatenation process of HR SGM features and LR global-wise features. Detailed structure of this module is presented in Fig. 4.

Through our experiments, we found that further extending MSRes Block to the shared encoder can make the performance of our framework even better. Hence, the final structure of our framework uses MSRes Block for both LR feature encoder and HR SGM feature extractor.

B3. Selective Cropping Algorithm. The appropriate approach to select the guidance patch from the HR image is also an important issue for model performance. There are mainly three types of cropping methods: random cropping, central cropping and selective cropping. Random cropping crops the HR patch in a random manner. Though this may select more discriminatory HR information for training, it can also lead to instability during testing. Central cropping always crops the central area of an image. It is the simplest and stablest way, but it includes less variety of attribute and information. In selective cropping, a patch with the richest contextual information is determined by selective search algorithm. Though it seems like having both the stability and variety of the former two methods, it also has a lower processing speed.

Algorithm 1 Selective Cropping

```

 $\{W, H, D\} \leftarrow \text{shape of the input } X$ 
 $c \leftarrow \{W/2, H/2, D/2\}$ 
 $L \leftarrow \sqrt{(W/2)^2 + (H/2)^2 + (D/2)^2}$ 
 $P_c \leftarrow \text{corresponding patch area with } c \text{ being center}$ 
 $V_{best} \leftarrow \text{var}(P_c) \# \text{var}() \text{ calculates the variance}$ 
 $P_{best} \leftarrow P_c$ 
 $dec\_count \leftarrow 0$ 
for  $r$  from  $L/6$  to  $L$  step  $L/6$ 
  for  $\vartheta$  from  $0$  to  $\pi$  step  $\pi/6$ 
    for  $\varphi$  from  $0$  to  $2\pi$  step  $\pi/3$ 
       $w \leftarrow r * \sin(\vartheta) + r * \cos(\varphi) + W/2$ 
       $h \leftarrow r * \sin(\vartheta) + r * \sin(\varphi) + H/2$ 
       $d \leftarrow r * \cos(\vartheta) + D/2$ 
       $c \leftarrow \{w, h, d\}$ 
      update  $P_c$ 
      if  $P_c$  extends outside  $X$ 
        return  $P_{best}$ 
      if  $\text{var}(P_c) > V_{best}$ 
         $V_{best} \leftarrow \text{var}(P_c)$ 
         $P_{best} \leftarrow P_c$ 
         $dec\_count \leftarrow 0$ 
      else
         $dec\_count \leftarrow dec\_count + 1$ 
      if  $dec\_count \geq 10$ 
        return  $P_{best}$ 

```

In our experiments, we find that selective cropping performs better than other approaches. To reduce the processing time, we designed a fast selective cropping algorithm. Selective cropping use the variance of a region to evaluate its information richness. Since most medical images has the object in the center, we start the search from the central area. The searching process is conducted on spherical coordinate system with fixed interval for the three axes r , ϑ and φ . For an image with size $W \times H \times D$, in every searching step, the coordinate can be converted to x , y and z axes of the orthogonal coordinate system using the following formulas:

$$\begin{cases} x = r * \sin(\vartheta) * \cos(\varphi) + W/2 \\ y = r * \sin(\vartheta) * \sin(\varphi) + H/2 \\ z = r * \cos(\vartheta) + D/2 \end{cases} \quad (9)$$

Note that the two coordinate systems have different origins (origin of the spherical coordinate system lies on the image center while origin of the orthogonal coordinate system is on the image corner), and for this reason we have to add $\frac{W}{2}$, $\frac{H}{2}$ and $\frac{D}{2}$ to each respective equation.

The exploration will gradually expand to the outer regions until it reaches the edges of the given image. The searching process will stop automatically if the algorithm finds the variance consistently decreases for 10 search areas. The brief procedure of our selective cropping algorithm is described with pseudo code in Algorithm 1. Note that the actual implementation includes more detailed operations to avoid repeated patch searching.

In our implementation, the HR guidance patch size is set to be 1/64 of the original HR image, so the extra memory cost it introduces can be very small. The HR guidance patch is essential in facilitating the SRT branch in doing self-supervised training. For this, we introduced a Self-Supervised Guidance Loss (SGL) to calculate the distance between the patch and the corresponding area of the SRT output. The loss function can be written as follows:

$$L_{sgl} = \frac{1}{N} \sum_{i=1}^N SIG(i) \cdot \|SRT(X \downarrow)_i - X_i\|^2, \quad (10)$$

where $SIG(i)$ is the signal function that returns 1 if i -th voxel is in the cropping window and 0 otherwise.

C. Task-Fusion Module

Despite the fact that the UST and SRT share an encoder, there is still scope for improvement in their interaction. Therefore, we propose the Task-Fusion Module (TFM) to constrain the outputs of these two tasks. For this module, we introduce both absolute and relative constraints. To identify an HR lesion region, the TFM module first computes the element-wise product of multitask learning network outputs (i.e., the predicted HR mask and generated HR image). This procedure can be stated as follows:

$$O_{fusion} = O_{srt} \otimes O_{ust}, \quad (11)$$

$$GT_{fusion} = X \otimes GT_{ust}, \quad (12)$$

where \otimes is the element-wise multiplication operation and GT_{ust} and GT_{fusion} are the segmentation label and the fused ground truth image for TFM.

Then, the module will calculate the absolute difference and relative difference between this product (i.e., O_{fusion}) and that of the ground truth segmentation label and HR image (i.e., GT_{fusion}). The absolute difference is expressed in the Target-Enhanced Loss (TEL), which calculates the average Euclidean distance between the target area voxels. It can be viewed as adding weights to the loss of segmentation area. As a result, SRT will pay more attention on the lesion area and UST will try to segment more precisely to avoid non-lesion area being calculated into TEL.

The relative difference is reflected in the Spatial Similarity Loss (SSL). Inspired by the Spatial Attention Mechanism in DANet [31], we compute the Self-Similarity Matrix of the element-wise product. Following that, we optimize the Frobenius norm of the subtraction of the Self-Similarity Matrix and the corresponding ground truth. The Self-Similarity Matrix mainly describes the pairwise relationships between voxels in a single image. To compute the Self-Similarity Matrix of a $D \times W \times H \times C$ image I , we first reshape it into $L \times C$, where $L = D \times W \times H$. By multiplying the $L \times C$ matrix with its transpose, we can have the final $L \times L$ matrix as the Self-Similarity Matrix. Because the TFM does not have any parameters, there will be no extra GPU memory cost. In the

end, TFM should also be removed along with the SRT during inference.

The loss function of TFM can be defined as follows.

$$L_{tfm} = L_{tel} + L_{ssl}, \quad (13)$$

$$L_{tel} = \frac{1}{N} \sum_{i=1}^N \|P_i \cdot SRT(X \downarrow)_i - y_i \cdot X_i\|^2, \quad (14)$$

$$L_{ssl} = \frac{1}{D^2 W^2 H^2} \sum_{i=1}^{D \cdot W \cdot H} \sum_{j=1}^{D \cdot W \cdot H} \|S_{ij}^{predict} - S_{ij}^{gt}\|^2, \quad (15)$$

$$S_{ij} = I_i \cdot I_j^T, \quad (16)$$

where P_i denotes the prediction of i -th voxel in O_{fusion} after binarization, and y_i represents its corresponding ground truth in GT_{fusion} . S_{ij} refers to the correlation between i -th and j -th voxel of the fusion feature I , while I_i represents the i -th voxel of the feature map.

D. Test Phase Fine-tuning

During clinical applications, segmentation models for medical images suffer from degradation in performance due to the generalization problem. The reason is that in real-world applications, the framework weights based on a specific dataset may be inappropriate for different patients. To enable the network's capacity to fit according to the test dataset distribution, we propose to use Test Phase Fine-tuning (TPF). Normally, we can directly deploy the learned model to make predictions on test samples after training. However, since the original HR images of testing dataset can be used as SRT ground truth, we can help the network better adapt to the distribution of testing dataset with such information.

One possible way of implementing TPF is by fixing the UST decoder parameters, then optimizing the SRT and encoder weights with LR and HR image pairs. This is a simple method, but it is particularly effective for improving encoder and SGM performance. But on the other hand, this may be harmful to the performance of UST, because SRT tends to become the primary task instead of the auxiliary one in this strategy. To overcome this difficulty, we introduce the use of pseudo-label for the UST task and fine-tune the framework using both tasks.

The use of pseudo labels make TPF looks similar to Semi-Supervised Learning. However, they are fundamentally different. Semi-Supervised Learning aims to make use of large quantity of unlabeled data for training, while TPF focuses on adapting the potential difference between the distributions of training and testing dataset. TPF also only updates network parameters with a small number of training epochs and a low learning rate to avoid drastically changes in network parameters. We also implemented TPF without pseudo labels in our experiments, however this strategy has relatively unstable performance as the priority shifts from UST to SRT. UST pseudo labels is mainly introduced to avoid such problem, rather than purely being the reference ground truth of UST.

A naive strategy is directly applying the labels to SRT and UST separately. Nevertheless, the performance can still be negatively affected by the potential errors in pseudo labels. so it would be better if we find a way to mitigate the negative influence of them. To mitigate such negative influence, we propose a simple yet effective strategy, that only use TFM for Test Phase Fine-tuning. TFM has the inherent characteristic that jointly takes account of SRT and UST labels. Since the SRT ground truth is absolutely correct, by fusing the pseudo UST label with it, we can balance out some of the errors in pseudo label. In our experiments, we use a learning rate of $1e^{-5}$ for all the methods, and only fine-tune the network with a single epoch. Results of the experiments suggest that using TFM-only strategy for TPF can lead to the best performance. Therefore, the final loss function used for TPF can be expressed as:

$$L_{tpf} = L_{tfm}, \quad (17)$$

with the ground truth being:

$$GT_{fusion} = X \otimes O_{ust}, \quad (18)$$

Note that X and O_{ust} are now the input image and UST output of the test dataset. Note that we need to firstly construct the ground truth labels (pseudo-labels) before using TPF.

E. Overall Objective Function

The overall loss function of our proposed patch-free segmentation framework is the linear combination of all the discussed losses, that is

$$L = L_{ust} + \omega_{srt}L_{srt} + \omega_{sgl}L_{sgl} + \omega_{tfm}L_{tfm}, \quad (19)$$

where ω_{srt} , ω_{tfm} and ω_{sgl} are hyper-parameters, and are all set to 0.5 by default. This objective function can be optimized end-to-end.

IV. EXPERIMENTS

A. Datasets and Evaluation Metrics

We used two datasets in our experiments. The first one is the publicly available BraTS2020 dataset [32], [33], [34], which contains a total number of 369 instances. This dataset focuses on brain tumors. For each subject, there are four modality MRI images (i.e., T1, T2, T1ce and FLAIR) and a ground truth segmentation mask. All the images have the size of $240 \times 240 \times 155$, and the spacing of $1\text{mm} \times 1\text{mm} \times 1\text{mm}$. The ground truth mask includes three classes, which are Tumor Core (TC), Enhanced Tumor (ET) and Whole Tumor (WT). For better usage, we removed the edges without brain part along x-axis and y-axis by 24 voxels, and finally resized all the images to size $192 \times 192 \times 128$.

Another dataset is a privately-owned liver segmentation dataset. This dataset is collected from a single center and contains 347 cases. For each case, there is a liver MRI image and a corresponding ground truth mask. The ground truth is carefully labeled by experienced doctors. Spacings of the images are

all regulated to $1.5\text{mm} \times 1.5\text{mm} \times 1.5\text{mm}$, and the sizes of the volumetric data vary around $250 \times 250 \times 140$. Similar to the pre-processing of BraTS2020 dataset, we omitted the slices without liver content and cropped the central $192 \times 192 \times 128$ area as the final images.

We employed three evaluation metrics in the experiment, which are Dice Similarity Coefficient (DSC), 95% Hausdorff Distance (HD95) and Jaccard Coefficient. DSC and Jaccard mainly focus on the segmentation area, while HD95 pays more attention to the segmentation boundaries. These three metrics provide a more comprehensive assessment of our method's effectiveness.

B. Implementation Details

We compared our method with other patch-based 3D segmentation methods and patch-free methods. For patch-based methods, we use sliding window strategy with a stride of 48, 48, 32 during inference. The patch-based methods used in our experiments are:

- 1) **3D UNet** [20]. Proposed in 2016, 3D UNet is widely used in many 3D segmentation tasks. It retains the iconic skip connection structure of the classic UNet. It can be viewed as a simple 3D modification of UNet with a less network width. It is named as UNet3D in the experimental results.
- 2) **3D Res-UNet** [29]. Proposed in 2017, 3D Res-UNet is the improved version of 3D UNet. For each encoder layer, it adds residual connections. This network shows better performance than 3D UNet in our experiments, and we build our framework base on it. It is labeled as ResUNet3D in the table.
- 3) **VNet** [21]. Proposed in 2017, VNet is a 3D segmentation model based on Encoder-Decoder structure. It keeps the skip connections structure and also introduces residual connections. But different from 3D UNet, it uses strided convolution for pooling. It uses fewer convolution operation for the shallow layers, and uses more of them for the deeper layers.

We also compared with some state-of-the-art patch-free methods in our experiments, which are:

- 1) **ResUNet3D \uparrow** . This method perform segmentation with a $2 \times$ down-sampled image. Then, it uses tricubic interpolation [26] algorithm to enlarge the output mask to the original size. It can be viewed as a naive patch-free method, but since it only conducts segmentation in a low-dimensional space, the performance may be inferior to other methods.
- 2) **ResUNet3D with Holistic Decomposition** [14]. Proposed in late 2019, Holistic Decomposition (HD) is the inverse operation of Sub-Pixel [27]. It can sub-sample a large 3D image into several small images without information loss. It can help lower the memory cost since it reduces the width and height of the feature maps. According to the paper, we set the down-shuffling factors to 2 for all three dimensions to achieve the best performance. It is labeled as HDResUNet in our experimental results.

TABLE I

COMPARISONS OF DIFFERENT GUIDANCE PATCH CROPPING METHODS ON BRATS2020. HD95 REFERS TO 95% HAUSDORFF DISTANCE.

Method	DSC (%)	HD95 (mm)	Jaccard (%)	Time (s)
Random Cropping	83.41	9.87	73.29	0.0126
Central Cropping	83.82	7.83	74.01	0.0126
Selective Cropping	84.13	8.33	74.38	0.0285

TABLE II

COMPARISONS OF DIFFERENT MSRES BLOCK APPLYING STRATEGIES. WE GRADUALLY REPLACE ORIGINAL RES BLOCK WITH MSRES BLOCK ON DIFFERENT MODULES TO TEST THE INFLUENCE OF THIS MODULE ON THE MODEL PERFORMANCE.

MSRes Applied Modules	DSC (%)	HD95 (mm)	Jaccard (%)	Memory (M)
w/o MSRes	84.13	8.33	74.38	9999
SGM w/ MSRes	84.15	8.42	74.47	10025
SGM+Encoder w/ MSRes	84.43	8.32	74.95	10693

- 3) **Point-Unet** [28]. In late 2021, Point-Unet proposed an alternative way of realizing 3D image segmentation by converting it into a point-cloud segmentation problem. The authors designed Context-Aware Sampling to simplify the input information and reduce the computational cost. This framework firstly uses a simple Saliency Attention Network (SAN) with the entire 3D image as input to coarsely locate the target. After that, it conducts point sampling according to the output attention map of SAN. Potential lesion area will be sampled at maximum density, while the rest areas simply employs random sampling. We sampled 365000 points for BRATS2020 and 800000 points for the liver datasets to use Point-Unet for the segmentation task.
- 4) **SAN** [28]. As aforementioned, SAN is used as a coarse segmentation network for Point-Unet. In compared to Point-Unet, it has a faster inference speed but at the expense of accuracy. Unlike our framework being a more universal method, Point-Unet is typically designed for datasets with small target segmentation areas. When applying Point-Unet to datasets with large target areas, its processing time and memory cost increase dramatically because more points are needed to be sampled. Therefore, we also compare the results for SAN in our experiments.

Except for Point-Unet, we implement all models with an NVIDIA GTX 1080Ti GPU. This graphical card has a total number of 11G video memory, which is insufficient for training a 3D UNet with $192 \times 192 \times 128$ input, but enough for our patch-free method. As to Point-Unet, when trained with batch size 1, it needs at least 16G video memory on BRATS2020, and at least 32G for the liver dataset due to the larger target areas. Hence, we used an NVIDIA GTX A6000 (48G) for its training. Inference time is calculated for all methods on the same machine with Intel Xeon CPU E5-2640 v4, 4×16G DDR4 2400MHz RAM and GTX 1080Ti GPU, running Ubuntu 16.04.3 LTS. The data augmentation

TABLE III

COMPARISONS OF DIFFERENT TPF METHODS ON BRATS2020. HD95 REFERS TO 95% HAUSDORFF DISTANCE. THE PRESENTED RESULTS ARE ACQUIRED WITH OR WITHOUT MSRES BLOCKS.

TPF Supervision Strategy	Res Block-based			MSRes Block-based		
	DSC (%)	HD95 (mm)	Jaccard (%)	DSC (%)	HD95 (mm)	Jaccard (%)
w/o TPF	84.13	8.33	74.38	84.43	8.32	74.95
TPF w/ SRT	84.10	8.32	74.33	84.30	8.90	74.67
TPF w/ SRT+UST	84.23	8.82	74.56	84.58	7.54	75.03
TPF w/ SRT+UST+TFM	84.55	8.33	74.38	84.81	7.98	75.45
TPF w/ TFM only	84.63	8.27	75.06	84.88	7.51	75.48

includes random flip, random rotation and random shift for all the methods. Random cropping is only used on patch-based methods. For all the methods, we used Instance Normalization and Leaky ReLU as it is recommended in [35].

For fair comparison, we set all the methods' input size to $96 \times 96 \times 64$ (except for HDResUNet and Point-Unet). Therefore, the input size of patch-based methods and patch-free methods can be the same. Specifically, HDResUNet uses the original image as input, but once the network receives the input, the HDC operator [14] will also process it into several $96 \times 96 \times 64$ images (8 in our experiment) in the first step. The guidance patch size for our method is $48 \times 48 \times 32$. For both datasets, we split 80% for training and 20% for testing. The batch size for all the methods is 1. All the models are optimized by Adam [36] with the initial learning rate set to 1e-4 (only Point-Unet starts at 1e-3). The learning rate will be divided by 10 if the training loss has not reduced over 10 epochs. The training is complete, if the maximum number of epochs is reached or the learning rate drops to 1e-7.

C. Network Investigations

Variants of Guidance Patch Cropping Methods. We investigated the different settings of guidance patch cropping strategy, i.e., random cropping, central cropping and selective cropping. The Experimental results are presented in TABLE I. As is shown, the test score of random cropping is the lowest. This is because the location of guidance patch varies too much during test, and some of them even do not have adequate HR information, causing instability. In contrast, central cropping achieves improved performance due to its great stability. By always cropping the central area, we can also guarantee that each patch contains enough HR information. For selective cropping, the result shows that it has the best performance among all the methods. Though the time cost is also a little higher, it does not affect the overall processing speed of our framework thanks to the selective cropping algorithm. Therefore, in the end we choose to use selective cropping for our framework.

Application Strategies of Multi-Scale Residual Blocks. To improve the network, we employ MSRes Block. The usage of different kernel sizes reduces the scale inconsistency between the various inputs (i.e. LR image and HR guidance patch). We tested two network structure with MSRes Block. The first one is to use MSRes Block only for the SGMs, while the encoder's

TABLE IV

ABLATION STUDY RESULTS ON BRATS2020. HD95 REFERS TO 95% HAUSDORFF DISTANCE. SELECTIVE CROPPING IS USED IN THE EXPERIMENT. MSRES BLOCK REFERS TO THE METHOD THAT SUBSTITUTES RES BLOCKS IN SGM AND THE SHARED ENCODER.

UST	SRT	TEL	SSL	SGM	MSRes	TPF	UNet3D			ResUNet3D		
							DSC (%)	HD95 (mm)	Jaccard (%)	Dice (%)	HD95 (mm)	Jaccard (%)
✓							80.58	10.56	70.21	81.83	8.88	71.75
✓	✓						81.71	9.64	71.15	82.09	8.41	71.52
✓	✓	✓					82.17	9.31	71.55	82.96	8.16	72.82
✓	✓	✓	✓				82.53	9.24	72.24	83.58	8.64	73.56
✓	✓	✓	✓	✓			82.99	8.75	73.03	84.13	8.33	74.38
✓	✓	✓	✓	✓	✓		83.28	8.56	73.29	84.43	8.32	74.95
✓	✓	✓	✓	✓	✓	✓	83.55	8.56	73.61	84.88	7.51	75.48

TABLE V

SEGMENTATION RESULTS ON TWO DATASETS. HD95 REFERS TO 95% HAUSDORFF DISTANCE, AND TIME DENOTES THE AVERAGE INFERENCE TIME FOR TWO DATASETS ON THE SAME MACHINE WITH A GTX 1080Ti.

Model	Patch-Free	End-to-End	BRATS2020			Liver Dataset			Time (s)	
			Dice (%)	HD95 (mm)	Jaccard (%)	Dice (%)	HD95 (mm)	Jaccard (%)		
V-Net [21]			✓	79.91	13.86	68.29	89.49	14.93	81.83	5.26
UNet3D [20]			✓	81.21	14.63	69.89	90.80	11.64	84.11	4.00
ResUNet3D [29]			✓	82.18	13.21	71.19	92.36	9.27	86.46	4.21
ResUNet3D \uparrow	✓	✓	✓	80.89	8.56	70.02	91.98	6.40	85.84	2.21
HDResUNet [14]	✓	✓	✓	82.45	9.21	72.07	92.88	5.58	87.33	0.19
SAN [28]	✓	✓	✓	81.50	9.46	70.71	92.33	5.98	86.28	1.65
Point-Unet [28]	✓	✓	✓	81.58	9.37	70.78	92.38	5.87	86.39	13.44
Ours (with TFM-TPF)	✓	✓	84.88	7.51	75.48	94.30	4.47	89.47	1.15	

convolution kernel size is fixed to 3 as usual. The scale of the extracted features by SGM tends to get closer to that of the encoder with this arrangement. Our experiment proves the effectiveness of such design, and the extra computational cost is nearly negligible due to the concise structure of SGM.

However, we speculate that a bidirectional design may have a better performance, so we further substitute the Res blocks of the shared encoder into MSRes Blocks. Under such network structure, the features from two input images can have an extra degree of freedom to meet a common scale, thus lead to a better flexibility. The results for these designs are shown in TABLE II. As is illustrated in the table, simply using MSRes Blocks for SGM only occupies 26M extra video memory, but the performance improvement is also very limited. In comparison, applying MSRes Block to both SGM and the shared encoder results in a considerable improvement, confirming our previous hypothesis.

Study of TPF Strategies. We tested four different TPF methods. The differences between these strategies are the modules that used in TPF process. The first strategy fixes the UST branch and only uses LR-HR image pairs for TPF, while the other three employ pseudo labels for UST and HR image as ground truth for the SRT to achieve a complete fine-tuning. The second TPF method directly optimize on the outputs of SRT and UST, while the third one furthermore involves TFM. The last one uses TFM-only strategy to mitigate the negative influence of potential errors in pseudo label. Same to the model training process, we also set a lower weight for SRT loss in TPF.

The experimental results of the four TPF methods is shown

in TABLE III. As is shown, the first strategy leads to a reduction in the performance of the UST due to the task priority shift. Pseudo-labels solve this problem, and as a result the other three strategies all gains improvements. Among these strategies, TFM-only performs best because it avoid the direct influence of the potential errors in pseudo labels. TFM combines the pseudo-labels with the genuine SRT ground truth (i.e. the HR image) to jointly optimize the framework, reducing the negative impact.

Component Effectiveness Analysis. In order to verify the effectiveness of the modules in our framework, we conducted an ablation study with our method on BraTS2020 dataset. Furthermore, we used two different backbones in the study, UNet3D and ResUNet3D, to make the results more convincing. The experimental results are shown in TABLE IV.

According the results in the Table IV, We can observe that using SRT as an auxiliary task improves the UST's capacity in reconstructing HR details. TFM and SGM also demonstrate their efficacy, increasing DSC by 1.49% and 0.24%, respectively. As the encoder is jointly tuned by the multi-task structure, TFM can adjust the parameters of the decoders simultaneously, boosting the segmentation performance. As to SGM, the effectiveness of it mainly lies in the HR representation it brings, which is useful for both SR and HR segmentation. We further tested MSRes Blocks and TPF in ablation study, and they also bring about improvements. The LR global-wise and HR guiding patch inputs are effectively adopted by MSRes Blocks. DSC accuracy is improved by 0.3% using this module. TPF aids in the adaption of the distribution test set, which shows a 0.4% rise. These well-

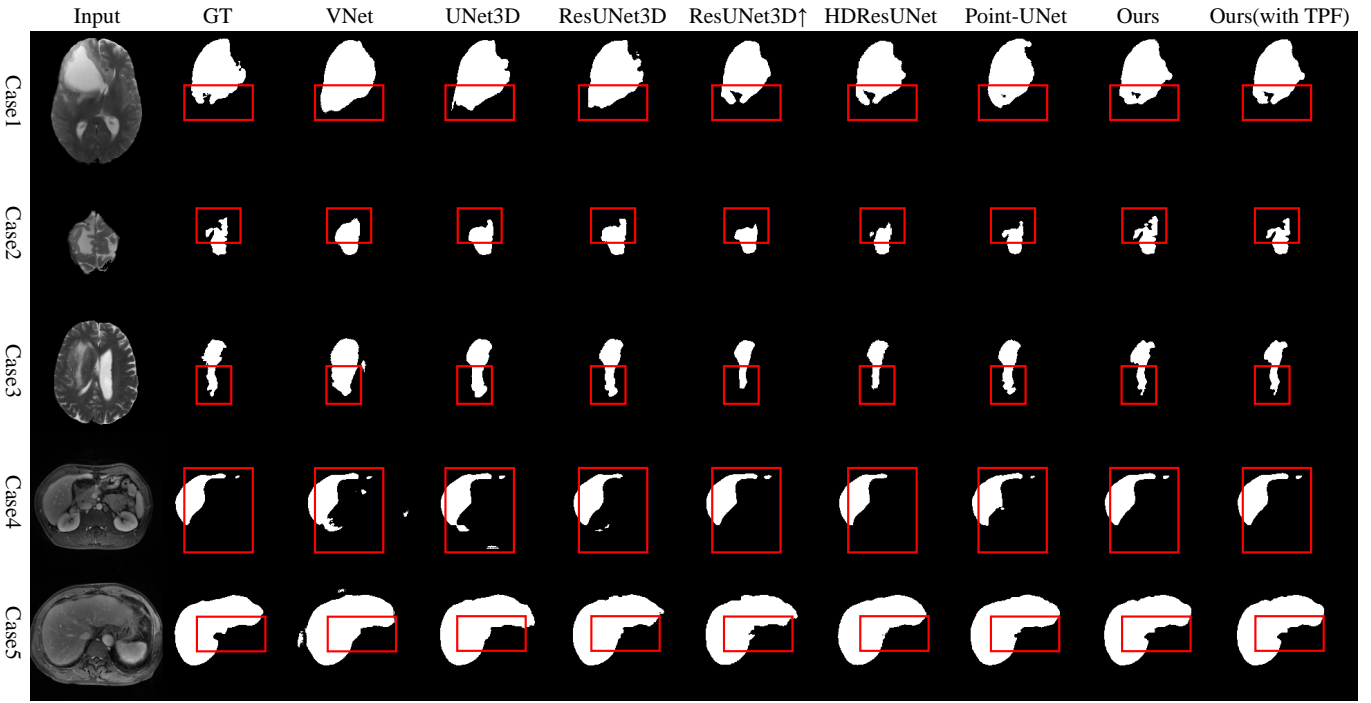


Fig. 5. Typical segmentation results of the experiment. Case1 to Case3 are from BRATS2020, while Case4 and Case5 are from the liver dataset. For the convenience of visualization, we only select one slice from every case. All the results are acquired with selective guidance cropping and TFM only TPF.

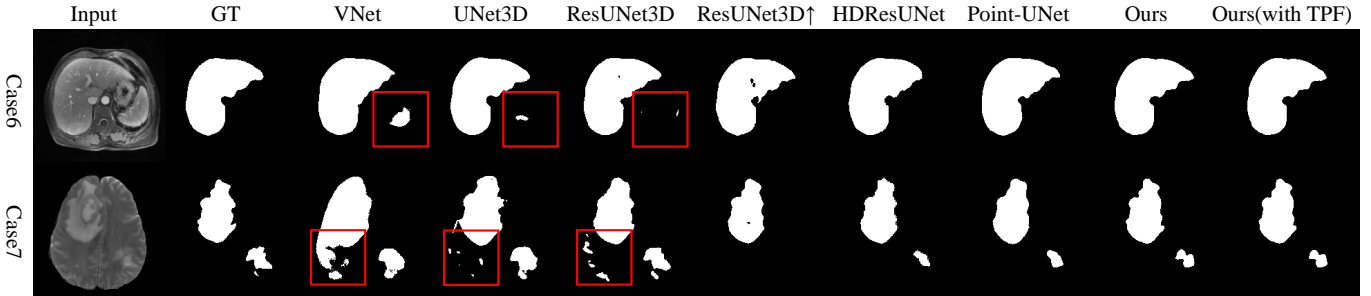


Fig. 6. Some example cases with more severe segmentation noise problem. Case6 is from the liver dataset while Case7 is from BRATS2020 dataset. As is shown, the segmentation noise problem only appears when using patch-based methods.

designed modules have a positive impact on the framework's performance. The best segmentation performance comes from combining these modules together.

D. Quantitative Comparison with Other Methods

The quantitative experimental results are summarized in TABLE V. Our framework outperforms traditional 3D patch-based models and other patch-free methods by a large margin on both datasets. When only keeps the main segmentation network, the inference speed of our methods is around 4 times higher than the patch-based methods.

Among all the patch-based methods, ResUNet3D has the best performance of 82.18% DSC on BRATS2020 and 92.36% DSC on the liver dataset. Our patch-free framework embedded on ResUNet3D achieves a 2.70% and 1.94% surge on these two datasets respectively. This proves the effectiveness of our method. HDRResUNet is another patch-free method based on ResUNet3D. Although it outperforms the patch-

based ResUNet3D on two datasets, it has lower performance in comparison to ours method. Compared with ResUNet3D↑, which only conducts segmentation in a low-dimensional space, our method demonstrates the need for HR feature restoration structures in the framework.

It also should be noted that on these two datasets, the simple patch-free method SAN achieves DSCs of 81.50% and 92.33%, which is superior than patch-based 3D UNet. The total amount of parameters in SAN is approximately 1.534M, which is less than a fifth of the 3D UNet. This demonstrates how important the global context is in enhancing network performance. Based on SAN, Point-Unet gains slight performance improvements. However, its memory cost is three times larger, and the inference speed is substantially slower.

E. Qualitative Analysis with Other Methods

Fig. 5 depicts some segmentation results of the experiments. According to the figure, noise and incorrect diagnosis are two

main limitations of patch-based approaches. Besides, some of the other patch-free models also expose their flaws, such as the detail loss caused by the high-frequency information loss. These cases are analyzed in detail one by one.

In Case 1, patch-based methods segment the lower area of the lesion incorrectly. It's a blurred area at the patch's boundary in the input image. As a result, patch-based methods fail to identify the lesion area. Because of the global contextual knowledge, this problem is solved in patch-free methods, leading to a better accuracy. This case also demonstrates TPF's usefulness, as TPF can fix certain minor errors.

Case 2 shows the inconsistency problem of patch-based methods, as patch-based methods tend to have sudden truncation on the edges of a patch. This problem is commonly seen when target area leaps over several patches, and we think this may be related with the padding technique in convolution neural networks. In [37], the authors point out that padding may result in artifacts on the edges of feature maps, and these artifacts may confuse the network. Luckily, in real life, most segmentation tasks do not involve objects on the edges, so this problem will not have much impact on the results. However, when patch-sampling is involved, then this may lead to significant performance degradation. That is also the reason why patch-free methods actually have the most obvious improvements in 95% Hausdorff Distance: with the global context, the model can more easily segment the target as a whole, thus making the segmentation edges smoother and more accurate. In our experiment, patch-free methods all successfully avoid the inconsistency problem, and among them, our framework has a better performance from all angles.

In Case 3, patch-based methods can only produce rough segmentation masks with insufficient details. This also has something to do with the inconsistency problem because the lesion area of Case 3 also overlaps several patches. As is explained above, there tend to be more errors on the patch edges, causing a less accurate segmentation result after fusion. In contrast, the result of our method is much more closer to the ground truth, and it should be noted that our method is the only one that find the tiny lesion extending outward at the bottom of the image.

Case 4 mainly illustrated the noise problem of patch-based methods. As is shown, patch-based methods are prone to producing segmentation noise in different region of the image. This problem mainly results from the limited context in patches. When conducting segmentation in a single patch, the model does not have the information of the real tumor area and it will be more likely to misdiagnose normal area as target. This problem has been observed many times in our experiments, and for some certain cases it can become extremely severe (the cases in Fig. 6 for example), leading to terrible segmentation result. Since there is no patches involved, patch-free methods all avoid such problem. But for HDResUNet, the unconnected liver part in the top right corner is missing in its output mask. This is because rather than using high-order interpolation to keep some high-frequency information, the HDC operator in Holistic Decomposition (HD) simply select voxels with a fixed spacing to form a sub-sampled output (which is similar to nearest neighbor interpolation), and such

practice will inevitably lead to high-frequency detail loss.

Case 5 is another case illustrating the inconsistency problem for patch-based methods. There is evident truncation in the emphasised areas of all the patch-based methods. The inconsistency causes uncertainty in the patch fusion process and lead to performance degradation. It should also be noted that we already use overlapped patches to mitigate such problem, and this problem could be even worse if used without overlapping. Our technique predicts segmentation masks that are substantially more qualitative and accurate.

V. CONCLUSION

In this paper, we present a new framework for fast and accurate patch-free segmentation that can capture global contextual information without adding too much computational cost. The framework can achieve HR segmentation with LR input by combining segmentation and SR in a multi-task structure. To capture the global context, we use entire LR images as the primary input, with an additional HR guidance patch to maintain certain HR local representations. We design a selective cropping algorithm and MSRes Block for selection of informative guidance patches and effective processing. We introduce TFM to combine the two tasks and exploit the advantage of their inter connections. Furthermore, we add Test Phase Fine-tuning (TPF) to improve the model's generalization ability. TPF can fine-tune the network parameters based on the distribution of test set by utilizing the test set HR images as SRT ground truth. We validate the framework's performance on two datasets to demonstrate its effectiveness. The result shows that it can efficiently generate better segmentation mask than other patch-based and patch-free methods with a very fast speed. As future work, we are going to incorporate a lightweight module [38] into the proposed method for further efficient computations.

ACKNOWLEDGMENTS

Authors would like to thank Mr.Rahul JAIN for his kind English proof.

REFERENCES

- [1] O. Ronneberger, P. Fischer, and T. Brox, "U-net: Convolutional networks for biomedical image segmentation," in *International Conference on Medical Image Computing and Computer-Assisted Intervention*. Springer, 2015, pp. 234–241.
- [2] P. F. Christ, M. E. A. Elshaer, F. Ettlinger, S. Tatavarty, M. Bickel, P. Bilic, M. Rempfler, M. Armbruster, F. Hofmann, M. D'Anastasi *et al.*, "Automatic liver and lesion segmentation in ct using cascaded fully convolutional neural networks and 3d conditional random fields," in *International Conference on Medical Image Computing and Computer-Assisted Intervention*. Springer, 2016, pp. 415–423.
- [3] Y. Tang, Y. Tang, Y. Zhu, J. Xiao, and R. M. Summers, "E2net: An edge enhanced network for accurate liver and tumor segmentation on ct scans," in *International Conference on Medical Image Computing and Computer-Assisted Intervention*. Springer, 2020, pp. 512–522.
- [4] H. Huang, L. Lin, R. Tong, H. Hu, Q. Zhang, Y. Iwamoto, X. Han, Y.-W. Chen, and J. Wu, "Unet 3+: A full-scale connected unet for medical image segmentation," in *ICASSP 2020-2020 IEEE International Conference on Acoustics, Speech and Signal Processing (ICASSP)*. IEEE, 2020, pp. 1055–1059.
- [5] H. Huang, H. Zheng, L. Lin, M. Cai, H. Hu, Q. Zhang, Q. Chen, Y. Iwamoto, X. Han, Y.-W. Chen *et al.*, "Medical image segmentation with deep atlas prior," *IEEE Transactions on Medical Imaging*, 2021.

- [6] Q. Shao, L. Gong, K. Ma, H. Liu, and Y. Zheng, "Attentive ct lesion detection using deep pyramid inference with multi-scale booster," in *International Conference on Medical Image Computing and Computer-Assisted Intervention*. Springer, 2019, pp. 301–309.
- [7] M. Zlocha, Q. Dou, and B. Glocker, "Improving retinanet for ct lesion detection with dense masks from weak recist labels," in *International Conference on Medical Image Computing and Computer-Assisted Intervention*. Springer, 2019, pp. 402–410.
- [8] Y. Wang, Y. Zhou, W. Shen, S. Park, E. K. Fishman, and A. L. Yuille, "Abdominal multi-organ segmentation with organ-attention networks and statistical fusion," *Medical Image Analysis*, vol. 55, pp. 88–102, 2019.
- [9] Y. Xia, D. Yang, Z. Yu, F. Liu, J. Cai, L. Yu, Z. Zhu, D. Xu, A. Yuille, and H. Roth, "Uncertainty-aware multi-view co-training for semi-supervised medical image segmentation and domain adaptation," *Medical Image Analysis*, vol. 65, p. 101766, 2020.
- [10] T. Kittrungrotsakul, X.-H. Han, Y. Iwamoto, L. Lin, A. H. Foruzan, W. Xiong, and Y.-W. Chen, "Vesselnet: A deep convolutional neural network with multi pathways for robust hepatic vessel segmentation," *Computerized Medical Imaging and Graphics*, vol. 75, pp. 74–83, 2019.
- [11] F. Madesta, R. Schmitz, T. Rösch, and R. Werner, "Widening the focus: Biomedical image segmentation challenges and the underestimated role of patch sampling and inference strategies," in *International Conference on Medical Image Computing and Computer-Assisted Intervention*. Springer, 2020, pp. 289–298.
- [12] Y. Tang, R. Gao, H. H. Lee, S. Han, Y. Chen, D. Gao, V. Nath, C. Bermudez, M. R. Savona, R. G. Abramson *et al.*, "High-resolution 3d abdominal segmentation with random patch network fusion," *Medical Image Analysis*, vol. 69, p. 101894, 2021.
- [13] H. Yang, C. Shan, A. Bouwman, A. F. Kolen, and P. H. de With, "Efficient and robust instrument segmentation in 3d ultrasound using patch-of-interest-fusenet with hybrid loss," *Medical Image Analysis*, vol. 67, p. 101842, 2021.
- [14] G. Zeng and G. Zheng, "Holistic decomposition convolution for effective semantic segmentation of medical volume images," *Medical Image Analysis*, vol. 57, pp. 149–164, 2019.
- [15] Y. Huang, L. Shao, and A. F. Frangi, "Simultaneous super-resolution and cross-modality synthesis of 3d medical images using weakly-supervised joint convolutional sparse coding," in *Proceedings of the IEEE Conference on Computer Vision and Pattern Recognition*, 2017, pp. 6070–6079.
- [16] L. Wang, D. Li, Y. Zhu, L. Tian, and Y. Shan, "Dual super-resolution learning for semantic segmentation," in *Proceedings of the IEEE/CVF Conference on Computer Vision and Pattern Recognition*, 2020, pp. 3774–3783.
- [17] H. Wang, L. Lin, H. Hu, Q. Chen, Y. Li, Y. Iwamoto, X.-H. Han, Y.-W. Chen, and R. Tong, "Patch-free 3d medical image segmentation driven by super-resolution technique and self-supervised guidance," in *International Conference on Medical Image Computing and Computer-Assisted Intervention*. Springer, 2021, pp. 131–141.
- [18] O. Oktay, J. Schlemper, L. L. Folgoc, M. Lee, M. Heinrich, K. Misawa, K. Mori, S. McDonagh, N. Y. Hammerla, B. Kainz *et al.*, "Attention u-net: Learning where to look for the pancreas," *arXiv preprint arXiv:1804.03999*, 2018.
- [19] L. Zhou, C. Zhang, and M. Wu, "D-linknet: Linknet with pretrained encoder and dilated convolution for high resolution satellite imagery road extraction," in *Proceedings of the IEEE Conference on Computer Vision and Pattern Recognition Workshops*, 2018, pp. 182–186.
- [20] Ö. Çiçek, A. Abdulkadir, S. S. Lienkamp, T. Brox, and O. Ronneberger, "3d u-net: learning dense volumetric segmentation from sparse annotation," in *International Conference on Medical Image Computing and Computer-Assisted Intervention*. Springer, 2016, pp. 424–432.
- [21] F. Milletari, N. Navab, and S.-A. Ahmadi, "V-net: Fully convolutional neural networks for volumetric medical image segmentation," in *2016 Fourth International Conference on 3D Vision (3DV)*. IEEE, 2016, pp. 565–571.
- [22] Q. Yu, D. Yang, H. Roth, Y. Bai, Y. Zhang, A. L. Yuille, and D. Xu, "C2fnas: Coarse-to-fine neural architecture search for 3d medical image segmentation," in *Proceedings of the IEEE/CVF Conference on Computer Vision and Pattern Recognition*, 2020, pp. 4126–4135.
- [23] Y. He, D. Yang, H. Roth, C. Zhao, and D. Xu, "Dints: Differentiable neural network topology search for 3d medical image segmentation," in *Proceedings of the IEEE/CVF Conference on Computer Vision and Pattern Recognition*, 2021, pp. 5841–5850.
- [24] H. Kim, J. Jung, J. Kim, B. Cho, J. Kwak, J. Y. Jang, S.-w. Lee, J.-G. Lee, and S. M. Yoon, "Abdominal multi-organ auto-segmentation using 3d-patch-based deep convolutional neural network," *Scientific Reports*, vol. 10, no. 1, pp. 1–9, 2020.
- [25] P.-Y. Kao, F. Shailja, J. Jiang, A. Zhang, A. Khan, J. W. Chen, and B. Manjunath, "Improving patch-based convolutional neural networks for mri brain tumor segmentation by leveraging location information," *Frontiers in Neuroscience*, vol. 13, p. 1449, 2020.
- [26] F. Lekien and J. Marsden, "Tricubic interpolation in three dimensions," *International Journal for Numerical Methods in Engineering*, vol. 63, no. 3, pp. 455–471, 2005.
- [27] W. Shi, J. Caballero, F. Huszar, J. Totz, A. P. Aitken, R. Bishop, D. Rueckert, and Z. Wang, "Real-time single image and video super-resolution using an efficient sub-pixel convolutional neural network," in *Proceedings of the IEEE Conference on Computer Vision and Pattern Recognition*, 2016, pp. 1874–1883.
- [28] N.-V. Ho, T. Nguyen, G.-H. Diep, N. Le, and B.-S. Hua, "Point-unet: A context-aware point-based neural network for volumetric segmentation," in *International Conference on Medical Image Computing and Computer-Assisted Intervention*. Springer, 2021, pp. 644–655.
- [29] L. Yu, X. Yang, H. Chen, J. Qin, and P. A. Heng, "Volumetric convnets with mixed residual connections for automated prostate segmentation from 3d mr images," in *Proceedings of the AAAI Conference on Artificial Intelligence*, vol. 31, no. 1, 2017.
- [30] K. He, X. Zhang, S. Ren, and J. Sun, "Deep residual learning for image recognition," in *Proceedings of the IEEE Conference on Computer Vision and Pattern Recognition*, 2016, pp. 770–778.
- [31] J. Fu, J. Liu, H. Tian, Y. Li, Y. Bao, Z. Fang, and H. Lu, "Dual attention network for scene segmentation," in *Proceedings of the IEEE/CVF Conference on Computer Vision and Pattern Recognition*, 2019, pp. 3146–3154.
- [32] S. Bakas, H. Akbari, A. Sotiras, M. Bilello, M. Rozycski, J. S. Kirby, J. B. Freymann, K. Farahani, and C. Davatzikos, "Advancing the cancer genome atlas glioma mri collections with expert segmentation labels and radiomic features," *Scientific Data*, vol. 4, no. 1, pp. 1–13, 2017.
- [33] S. Bakas, M. Reyes, A. Jakab, S. Bauer, M. Rempfler, A. Crimi, R. T. Shinohara, C. Berger, S. M. Ha, M. Rozycski *et al.*, "Identifying the best machine learning algorithms for brain tumor segmentation, progression assessment, and overall survival prediction in the brats challenge," *arXiv preprint arXiv:1811.02629*, 2018.
- [34] B. H. Menze, A. Jakab, S. Bauer, J. Kalpathy-Cramer, K. Farahani, J. Kirby, Y. Burren, N. Porz, J. Slotboom, R. Wiest *et al.*, "The multimodal brain tumor image segmentation benchmark (brats)," *IEEE Transactions on Medical Imaging*, vol. 34, no. 10, pp. 1993–2024, 2014.
- [35] F. Isensee, P. Kickingereder, W. Wick, M. Bendszus, and K. H. Maier-Hein, "No new-net," in *International MICCAI Brainlesion Workshop*. Springer, 2018, pp. 234–244.
- [36] D. P. Kingma and J. Ba, "Adam: A method for stochastic optimization," in *International Conference on Learning Representations*, 2015.
- [37] B. Alsallakh, N. Kokhlikyan, V. Miglani, J. Yuan, and O. Reblitz-Richardson, "Mind the pad – cnns can develop blind spots," in *International Conference on Learning Representations*, 2021. [Online]. Available: <https://openreview.net/forum?id=m1CD7tPubNy>
- [38] Y. Li, Y. Iwamoto, L. Lin, R. Xu, R. Tong, and Y.-W. Chen, "Volumenet: A lightweight parallel network for super-resolution of mr and ct volumetric data," *IEEE Transactions on Image Processing*, vol. 30, pp. 4840–4854, 2021.



Hongyi Wang was born in Nanjing, China, in 1998. He received the B.E. degree in computer science and technology from Harbin Institute of Technology, Harbin, China, in 2020. He is currently pursuing the Ph.D. degree from the College of Computer Science and Technology, Zhejiang University, China. His research interests include medical image processing and analysis, super-resolution, and deep learning.



Yutaro Iwamoto (Member, IEEE) received the B.E., M.E., and D.E. degrees from Ritsumeikan University, Kusatsu, Japan, in 2011, 2013, and 2017, respectively. He is currently an Assistant Professor with Ritsumeikan University. His current research interests include medical image processing, computer vision, and deep learning.



Lanfen Lin (Member, IEEE) received the B.S. and Ph.D. degrees in aircraft manufacture engineering from Northwestern Polytechnical University in 1990 and 1995, respectively. She held a postdoctoral position with the College of Computer Science and Technology, Zhejiang University, China, from January 1996 to December 1997. She is currently a Full Professor and the Vice Director of the Artificial Intelligence Institute, Zhejiang University. Her research interests include medical image processing, big data analysis, and data mining.



Xian-Hua Han (Member, IEEE) received a B.E. degree from Chongqing University, Chongqing, China, a M.E. degree from Shandong University, Jinan, China, a D.E. degree in 2005, from the University of Ryukyus, Okinawa, Japan. From April 2007 to March 2013, she was a postdoctoral fellow and an associate professor with College of Information Science and Engineering, Ritsumeikan University, Shiga, Japan. From April 2016 to March 2017, she was a senior researcher with the Artificial Intelligence Research Center, National Institute of Advanced Industrial Science and Technology, Japan. She is currently an associate Professor with the Artificial Intelligence Research Center, Yamaguchi University, Japan. Her current research interests include image processing and analysis, pattern recognition, machine learning, computer vision and hyperspectral image analysis. She is a member of the IEEE, IEICE.



Hongjie Hu, Ph.D., a chief physician and doctoral supervisor in Department of Radiology, Sir Run Run Shaw hospital, Zhejiang University school of medicine since 2015. He has engaged in medical imaging for over 30 years. He achieved his master's degree of medicine (1992) and doctor's degree of medicine (1998) in Zhejiang Medical University. He went to some place for further education at Loma Linda University medical center in 2000, Myo clinic in 2008 and Cleveland University clinic in USA. He has rich clinical experience in cardiothoracic diagnosis and interventional radiotherapy.



Yen-Wei Chen (Member, IEEE) received the B.E. degree from Kobe University, Kobe, Japan, in 1985, and the M.E. and D.E. degrees from Osaka University, Osaka, Japan, in 1987 and 1990, respectively. From 1991 to 1994, he was a Research Fellow with the Institute for Laser Technology, Osaka. From October 1994 to March 2004, he was an Associate Professor and a Professor with the Department of Electrical and Electronic Engineering, University of the Ryukyus, Okinawa, Japan. He is currently a Professor with the College of Information Science and Engineering, Ritsumeikan University, Kyoto, Japan. He is also a Visiting Professor with the College of Computer Science and Technology, Zhejiang University, China, and the Research Center for Healthcare Data Science, Zhejiang Laboratory, China. His research interests include pattern recognition, image processing, and machine learning. He has published more than 200 research articles in these fields. He is an Associate Editor of the *International Journal of Image and Graphics* (IJIG) and an Associate Editor of the *International Journal of Knowledge-Based and Intelligent Engineering Systems*.



Qingqing Chen was born in Wenzhou, China in 1993. She got her doctor's degree in medicine from Zhejiang University in 2021, and now she is working at Sir Run Run Shaw Hospital, Zhejiang University School of Medicine, China. Her research mainly focuses on the artificial intelligence of liver imaging, such as lesion classification, LI-RADS category, prediction or prognosis of HCC and et al. She made presentation at Radiology Society of North America (RSNA 2017) in Chicago and received a short-term exchange to Department of Information Science and Engineering of Ritsumeikan University for three months.



Ruofeng Tong received the Ph.D. degree from the Applied Mathematics Department, Zhejiang University, China, in 1996. He is currently a Professor with the Computer Science Department, Zhejiang University. His research interests include image and video processing, computer graphics, and computer aided diagnosis.



Yinhao Li received the B.E. degree from Southeast University Chengxian College, Nanjing, China, in 2013, and the M.E. and D.E. degrees from Ritsumeikan University, Kusatsu, Japan, in 2018 and 2021, respectively. He is currently a Postdoctoral Researcher with the Research Center for Healthcare Data Science, Zhejiang Laboratory, China. His research interests include image processing and analysis, super-resolution, and deep learning. He was a recipient of the IEEE CE East Japan Chapter ICCE Young Scientist Paper Award in 2018, and the Japan Society for the Promotion of Science (JSPS) Research Fellowship for Young Scientists in 2019.